$$\int_0^\infty P(\tau_D)d\tau_D = 1 \qquad (2)$$

$T_f(\tau)$, $T_s(\tau)$, and $\theta(x)$ are defined as:

$$T_f(\tau) = \frac{1 - F_f + F_f \exp(-\tau/\tau_{Tf})}{1 - F_f}$$
$$T_s(\tau) = \frac{1 - F_s + F_s \exp(-\tau/\tau_{Ts})}{1 - F_s} \qquad (3)$$

$$\theta(x) = \begin{cases} 1 & (x > 0) \\ 0 & (x < 0) \end{cases} \qquad (4)$$

where τ_{Tf} and F_f are the triplet time and the triplet fraction for the fast-diffusing assembly (τ_{Ts} and F_s for the slow-diffusing assembly), respectively. Although the original model assumes all assemblies are in the same triplet state (7), it is known that the same fluorescent molecule gives a different triplet time and triplet fraction dependent on its environment (7,8). Because of their differences in size and structure, the fluorophores in the fast-diffusing assembly and in the slow-diffusing assemblies are considered to be exposed to different environments. We therefore set two kinds of triplet time and triplet fraction here.

Using CONTIN (5,6) combined with least-squares fitting, the approximate solution of $P(\tau_D)$ was calculated from $G_{exp}(\tau)$ for each set of triplet fractions (F_f and F_s, where F_i = 0.01, 0.02, ..., 1.0 (i= f or s)) and for the triplet time for the slow diffusing assembly τ_{Ts}. Here, τ_{Ts} was varied over the time range near τ_{Tf} (from 0.1 μs to 10 μs). This is because τ_{Ts} was found to fit only the time range near τ_{Tf}, which seems reasonable from direct observations of the rate of the triplet decay k_T and of the intersystem crossing k_{ISC} of rhodamine 6G in different environments (7,9). We note that the triplet time τ_{Ts} satisfies $(k_{ISC} + k_T)^{-1} < \tau_{Ts} < k_T^{-1}$ for $k_{10} > k_T$ where k_{10} is the depopulation rate of the first singlet excited state S_1 to the ground state S_0 (see scheme at right). While τ_{Ts} was varied, the triplet time for the fast diffusing assembly τ_{Tf} was assumed to be the same as that of TMR (2.40 μs based on the relation between τ_{Tf} and the laser power (8)). The calculated autocorrelation function $G_{calc}(\tau)$ was obtained from $P(\tau_D)$ using Equation (1). For each set of triplet fractions and τ_{Ts}, the chi-square (χ^2) value was calculated between $G_{exp}(\tau)$ and $G_{calc}(\tau)$, and the set that gave the minimum χ^2 value was selected under the condition 8 kDa < M_1 < 15 kDa, because M_1 represents the mass of the fast-diffusing, low-order Aβ assembly (dimers or trimers). We set ξ to 0.2 ms so that ξ may represent τ_D at the minimum in $P(\tau_D)$ between the peak of the fast-diffusing, low-order Aβ assembly and that of the slow-diffusing, high-order Aβ assembly.

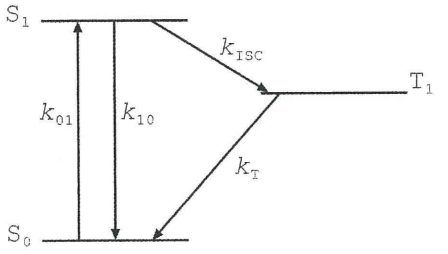

The average diffusion time of each i-th peak of $P(\tau_D)$ was determined by:

$$\tau_{D,i} = \int_{\tau_{D,i}^{min}}^{\tau_{D,i}^{max}} \tau_D P(\tau_D)\, d\tau_D \Big/ \int_{\tau_{D,i}^{min}}^{\tau_{D,i}^{max}} P(\tau_D)\, d\tau_D \quad (i = 1, 2, \ldots) \qquad (5)$$

where $\tau_{D,i}^{max}$ and $\tau_{D,i}^{min}$ represent the maximum and minimum diffusion time of each i-th peak of $P(\tau_D)$, respectively. τ_D is related to the cross-section of the confocal volume element and the diffusion coefficient D, and is given by:

Downloaded from www.jbc.org at Kyoto University, on March 28, 2011

$$\tau_D = \frac{w^2}{4D} \qquad (6)$$

where w is radial length of the confocal volume element. With the assumption that the studied species are spherical (which we confirmed using TEM or *in situ* AFM), the hydrodynamic radius R_h can be obtained from the Stokes-Einstein equation:

$$D = \frac{kT}{6\pi\eta R_h} \qquad (7)$$

where η is the solvent viscosity, k is Boltzmann's constant, and T is the absolute temperature. In the case of spherical structures, the mass M is proportional to R_h^3. Therefore, if a reference molecule with a known mass is measured, M of the studied species can be obtained as follows:

$$M = \left(\frac{\tau_D}{\tau_{D\,\mathrm{Reference}}}\right)^3 M_{\mathrm{Reference}} \qquad (8)$$

In the case of non-spherical structures, by measuring a reference with known diffusion coefficient $D_{\mathrm{Reference}}$, D of the studied species is obtained as follows:

$$D = \left(\frac{\tau_{D\,\mathrm{Reference}}}{\tau_D}\right) D_{\mathrm{Reference}} \qquad (9)$$

The relative abundance of each assembly was obtained by integrating each i-th peak of $P(\tau_D)$.

In Figs. 1*B*, 2*C*, 3*B*, and 3*C*, the distribution of assembly mass (log scale) or diffusion coefficient (log scale) is shown. To show the distribution in the graphs with the logarithmic scale on the abscissa, we newly introduced two parameters, $\tilde{M}$ (=log M) and $\tilde{D}$ (=log D) and transformed $P(\tau_D)$ either into $\tilde{P}(\tilde{M})$ (the distribution function of $\tilde{M}$) or $\overline{P}(\tilde{D})$ (the distribution function of $\tilde{D}$), where $\tilde{P}(\tilde{M})$ and $\overline{P}(\tilde{D})$ satisfy the following normalization conditions,

$$\int_0^\infty \tilde{P}(\tilde{M})d\tilde{M} = 1 \qquad (10)$$

$$\int_0^\infty \overline{P}(\tilde{D})d\tilde{D} = 1 \qquad (11)$$

These transformations are performed according to the following equations,

$$\tilde{P}(\tilde{M}) = \frac{1}{3}P(\tau_D)\tau_D \log_e 10 \qquad (12)$$

$$\overline{P}(\tilde{D}) = -P(\tau_D)\tau_D \log_e 10 \qquad (13)$$

$\tilde{P}(\tilde{M})$ (Figs. 1*B*, 2C, 3B&C) or $\overline{P}(\tilde{D})$ (Supplemental Fig. S7) is shown in the graphs.

In FCS measurements, the contribution of each component to the correlation curve is related to both relative abundance and relative brightness (10). If all components have equal brightness, the relative abundance of each assembly can be obtained by integrating each i-th peak of $P(\tau_D)$. This is true for ASPDs and early fibril intermediates, but not for fibrils containing more than one fluorophore. In the latter case, a rough estimate of the apparent relative abundance of the fibrils was obtained by integrating the i-th peak of $P(\tau_D)$(for details, see "*In situ monitoring of fibril formation*"). To confirm the rough estimates thus obtained, mature fibrils were separated in the retentate fractions of 0.1-μm filters (confirmed using TEM) and their amount was directly obtained from the fluorescence count using a fluorometer (Twinkle LB970; Berthold Technologies GmbH).

Analysis of FCS data obtained from immunoprecipitation eluates- As described above, the immunoisolated ASPDs were measured in highly viscid Gentle Elution Buffer (GEB; Pierce). As shown below, although the GEB itself does not contain fluorescent components, noisy signals were observed in a

Downloaded from www.jbc.org at Kyoto University, on March 28, 2011

very fast diffusion time range ($\tau < 0.01$ ms) of $G_{exp}(\tau)$ with samples in the GEB (either Alexa Fluor 532 or ASPDs). Such noisy signals were absent in $G_{exp}(\tau)$ with samples in 0.5X PBS. Although we do not know why the signal in the fast time range of $G_{exp}(\tau)$ was noisy, we believe that quenching of the fluorescence of the Alexa Fluor 532 dye in the GEB could lead to an increase in background noise, causing noisy signals at very fast diffusion time, because we found that the count per molecule of Alexa Fluor 532 in the GEB was about a tenth lower than that of Alexa Fluor 532 in 0.5X PBS. Because these noisy signals were indistinguishable from triplet signals, we only analyzed $G_{exp}(\tau)$ in a slow diffusion time range ($\tau > 1.0$ ms) for the immunoisolated ASPDs (the diffusion time of Alexa Fluor 532 dye in the GEB was ~0.43 ms). In this time range, the effect of the triplets was negligible; thus, the following equation of the original triplet-free model was used (11).

$$G_{exp}(\tau)_{GEB} = 1 + A\int_0^\infty \frac{1}{\left(1+\frac{\tau}{\tau_D}\right)\sqrt{\left(1+\frac{\tau}{s^2\tau_D}\right)}} P(\tau_D)\, d\tau_D \qquad (14)$$

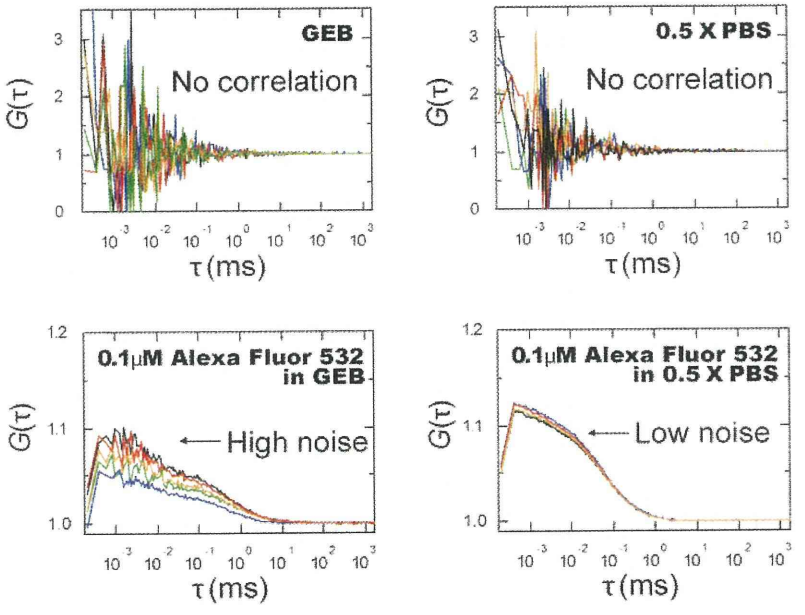

Toxicity assays- The Animal Care and Experimentation Committee of Mitsubishi Kagaku Institute of Life Sciences and Kyoto University approved all animal experiments. Primary cultures from rat septum regions, which include septal and basal forebrain cholinergic neurons, were prepared as described (1) and plated at a density of 2.4 x 10^5 cells/cm^2 on a poly-L-lysine (0.01%; Nacalai Tesque 28360-14)-coated 48-well plastic plates (0.3 ml/well). After 50-55 hrs, the medium was replaced with a serum-free neurobasal media containing B27 supplements, 0.5 mM L-glutamine, and 50 μg/ml gentamicin. After an additional 5 days of culture, the cells were treated with ASPD samples. Primary rat hippocampal cultures

Downloaded from www.jbc.org at Kyoto University, on March 28, 2011

were prepared (4) and plated at a density of 3.6 x 10^4 cells/cm^2 (48-well plastic plates) on a polyethyleneimine (0.02% PEI; Sigma P3143)-coated wells in neurobasal media containing B27 supplements and 2.5 μM L-glutamine. Cultures were maintained in this medium for a week. Then, approximately half of the medium was replaced once a week with neurobasal media containing B27 supplements, 2.0 μM L-glutamine, and 10% (v/v) astrocyte-derived conditioned medium (Sumitomo Bakelite Co., Ltd. MB-X9501). For the toxicity evaluation, apoptosis was determined quantitatively by monitoring cytoplasmic histone-associated DNA fragments with sandwich ELISA (Cell Death Detection ELISAplus, Roche Diagnostics), according to the manufacturer's instructions. The cells were treated with ASPD samples at 19-20 *days in vitro*. The apoptotic activity was expressed as absorbance difference (A_{405}-A_{450}) normalized by the amount of Aβ present. Alternatively, toxicity was also estimated by monitoring lactate dehydrogenase (LDH) activity in the culture supernate, which reflects plasma membrane damage, using Cytotoxicity Detection Kitplus (Roche Diagnostics) essentially according to the manufacturer's instructions. The toxicity was expressed as absorbance difference (A_{490}-A_{655}) normalized by the amount of Aβ present.

Statistics- The statistical significance of the differences among groups was determined by applying Games-Howell or Scheffé *post hoc* tests using StatView® 5.0 (SAS Institute Inc., Cary, NC, USA).

Downloaded from www.jbc.org at Kyoto University, on March 28, 2011

Table S1. Characteristics of ASD Antibodies and Anti-pan Aβ Antibodies

Antibody	Preference among Aβ types in dot blotting	K_d for ASPDs (nM)	Epitope map	Response to APP in dot blotting	Response to fibrils in immuno-TEM	Blockade of ASPD toxicity
rpASD1	ASPD	0.005	Several regions[a]	-	-	+
haASD1	ASPD	0.0005	Could not be determined[b]	-	-	-
6E10	All types	0.2	Aβ5-9[c]	+	+	-
82E1	All types	nd	Aβ1-5[c]	-	*nd*	-

nd; not determined.

The characteristics of ASPD-specific antibodies (upper two rows) used in this work and commercially available anti-pan Aβ antibodies (lower two rows) are summarized. The original data are from our previous report (2). [a]The binding of rpASD1 to synthetic-ASPDs was most strongly inhibited by N-terminal pentapeptides of Aβ. In addition, the binding was also inhibited by specific sets of non-N-terminal pentapeptides. The data suggest that different Aβ regions exist in close proximity to form the ASPD-specific epitope. [b]The binding of haASD1 to synthetic-ASPDs was not inhibited by the addition of any pentapeptide, suggesting that haASD1 recognizes a non-linear epitope formed by non-contiguous Aβ regions. [c]For 6E10 and 82E1, which did not discriminate ASPDs from other types of Aβ, complete inhibition was attained with a single pentapeptide in each case.

Downloaded from www.jbc.org at Kyoto University, on March 28, 2011

Fig. S1 Matsumura et al.

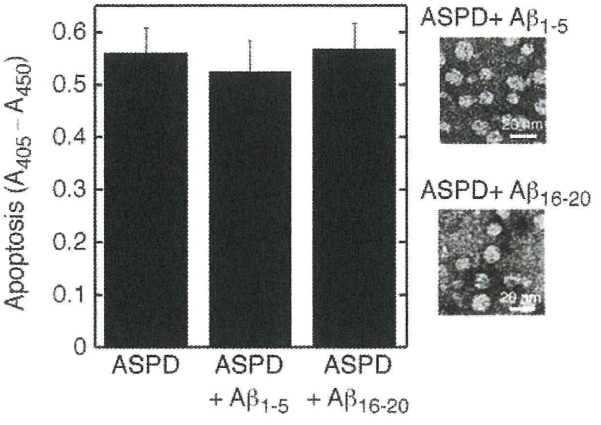

Supplemental Fig. S1. Excess amounts of $A\beta_{1-5}$ (DAEFR) or $A\beta_{16-20}$ (KLVFF) did not block toxic ASPD formation. ASPDs were prepared *in vitro* from 50 μM solutions of $A\beta_{1-42}$ using the slow rotation method (1) with or without a 10-fold molar excess of $A\beta_{1-5}$ or $A\beta_{16-20}$. Apoptotic activity against rat primary septal neuronal cultures was determined quantitatively by monitoring DNA fragmentation (n=18; see Additional Experimental Procedures). We also confirmed the presence of ASPDs using TEM (right panels). Neither $A\beta_{1-5}$ nor $A\beta_{16-20}$ affected the formation of toxic ASPDs.

Downloaded from www.jbc.org at Kyoto University, on March 28, 2011

Fig. S2 Matsumura et al.

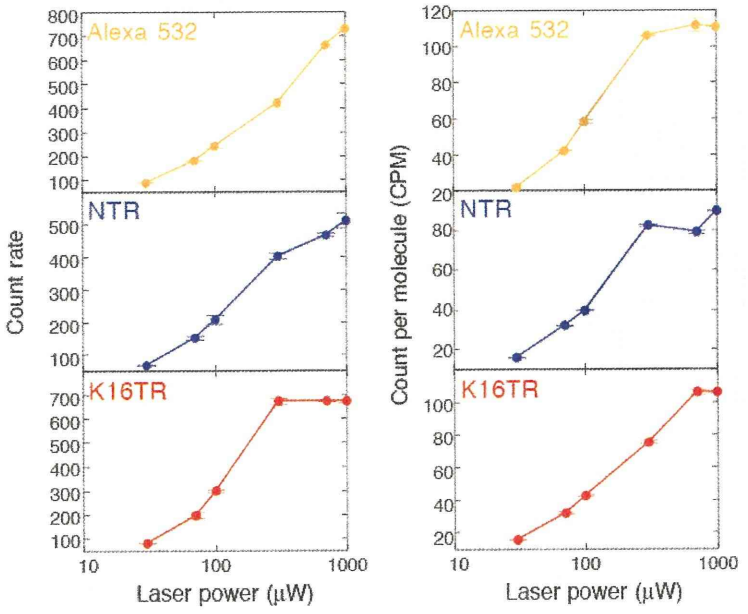

Supplemental Fig. S2. Optimization of laser power (intensity) for fluorescent probes. Since too strong a laser power saturates fluorescence absorption, while too weak a laser power results in a low signal-to-background ratio, NTR and K16TR (freshly dissolved at 0.05 μM in 0.5X PBS) were examined using FCS at various laser intensities. Between 30 and 300 μW, both the average photon number/sec (the count rate) and the count rate/ number of fluorescent molecules in a confocal volume (the count per molecule) increased with increasing laser power (n = 5). Therefore, we routinely set the laser power at 100 μW, which gave a high signal-to-background ratio (>100:1).

Downloaded from www.jbc.org at Kyoto University, on March 28, 2011

Fig. S3 Matsumura et al.

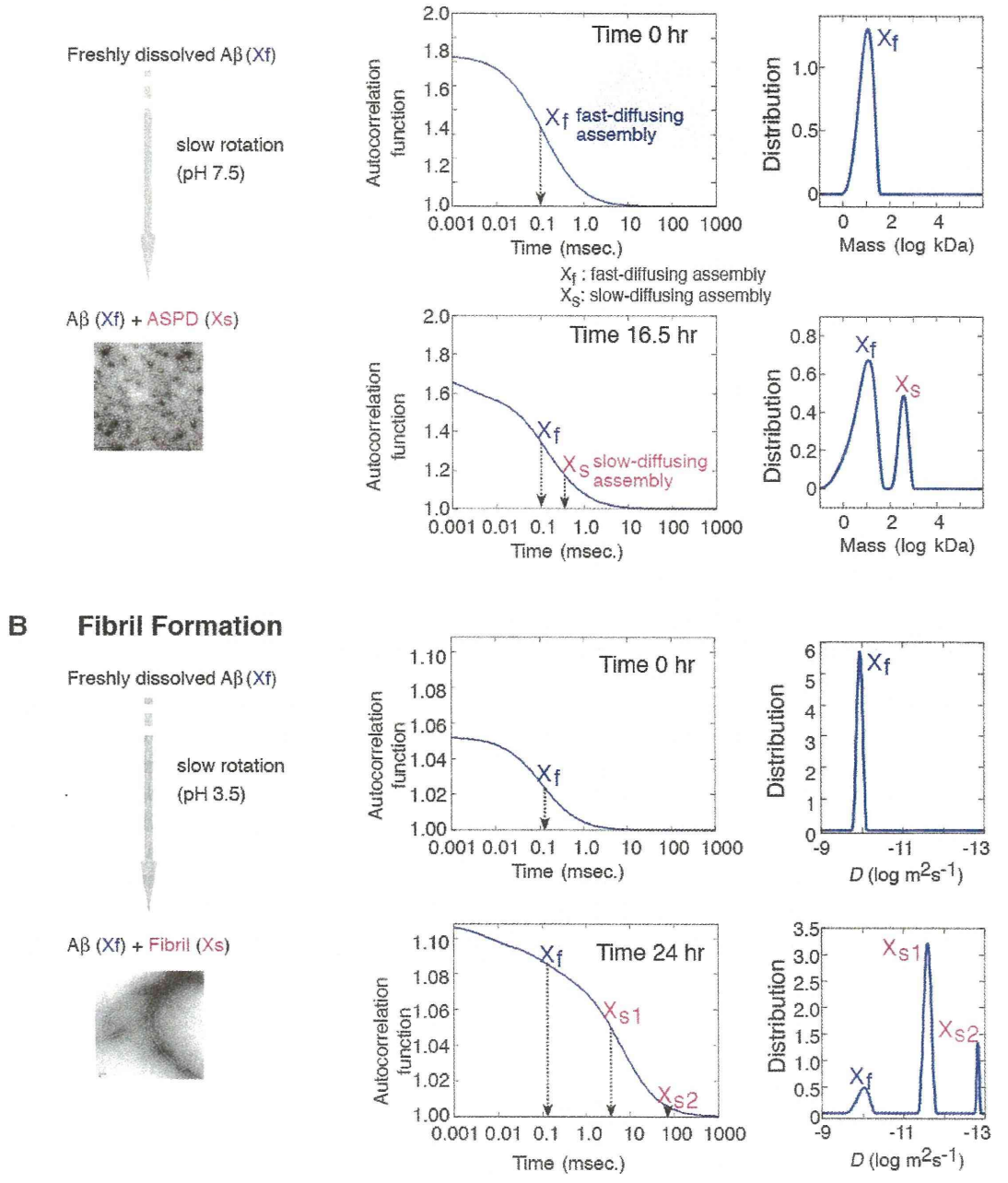

Supplemental Fig. S3. Evaluation of Aβ assembly processes into ASPDs or fibrils using TEM and FCS analyses. Analyses of ASPD formation (*A*) and fibril formation (*B*) (details in Experimental Procederes). Fibril formation is shown in apparent mass in Fig. 3 and in *D* in Fig. S7.

Downloaded from www.jbc.org at Kyoto University, on March 28, 2011

Fig. S4 Matsumura et al.

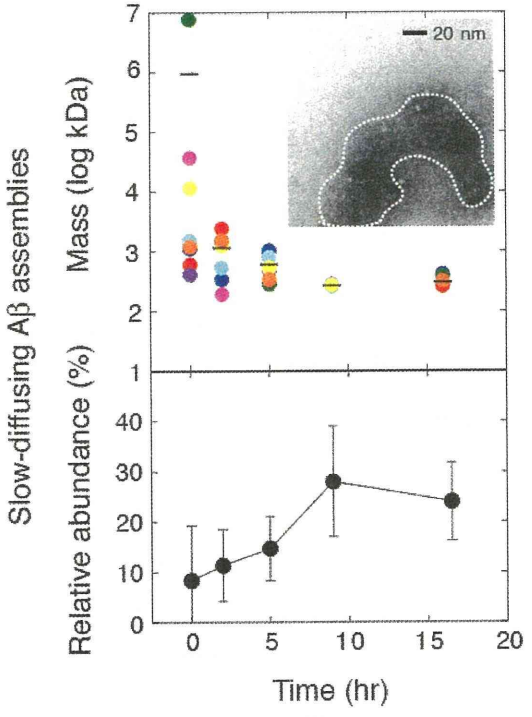

Supplemental Fig. S4. Time-dependent changes in mass and relative abundance of the slow-diffusing assemblies that appeared during ASPD formation. Each colored dot in the upper panel represents the mass of the slow-diffusing assemblies detected at the indicated time during the course of ASPD formation in a series of independent experiments (n = 8), and each bar represents the average mass at the indicated time. The average relative abundance of these assemblies is shown in the lower panel. Aβ trimers were the dominant species during the first 2 hrs of slow rotation. However, small amounts of slow-diffusing species with variable mass and relative abundance were detected reproducibly at these time points. Cloud-like uranyl acetate-stained structures (dotted line in *Inset*), clearly distinct from the staining of buffer-derived salts, were observed in low levels by TEM during the first 2 hrs of slow rotation, and we speculate that these species might be metastable and be destroyed during the sample preparation for TEM. It is unlikely that all of these species represent insufficiently dissolved Aβ (amorphous structure in Fig. 1B, arrow) because at 2 hrs, such amorphous structures were decreased in TEM, while these species were increased in FCS.

Downloaded from www.jbc.org at Kyoto University, on March 28, 2011

Fig. S5 Matsumura et al.

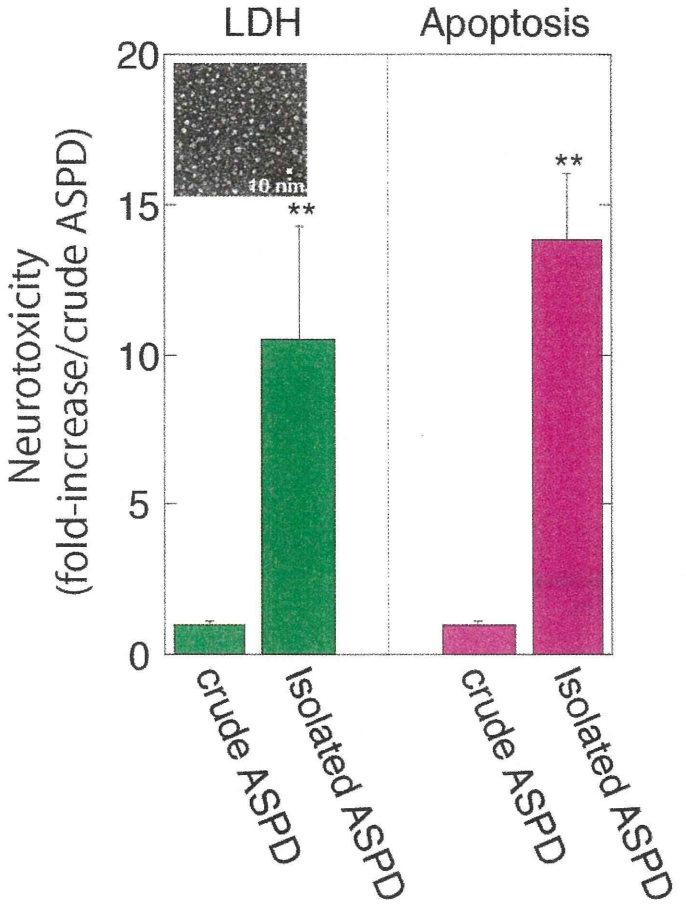

Supplemental Fig. S5. Neurotoxicity of the purified ASPDs. Neurotoxicity of the most toxic ASPDs immunoisolated by anti-ASPD haASD1 antibody was compared with that of crude ASPDs either by LDH release assay (monitoring plasma membrane damage) or by apoptotic activity assay (monitoring DNA fragmentation) according to the manufacturer's instructions using hippocampal rat primary neuronal cultures at 19 days *in vitro*. Specific activities of the isolated ASPDs are shown as fold-increase against those of the crude ASPDs (mean ± SD; Scheffé *post-hoc* test, **, $p < 0.001$, $n > 4$). The TEM image of the isolated ASPDs is shown in the inset.

Downloaded from www.jbc.org at Kyoto University, on March 28, 2011

Fig. S6 Matsumura et al.

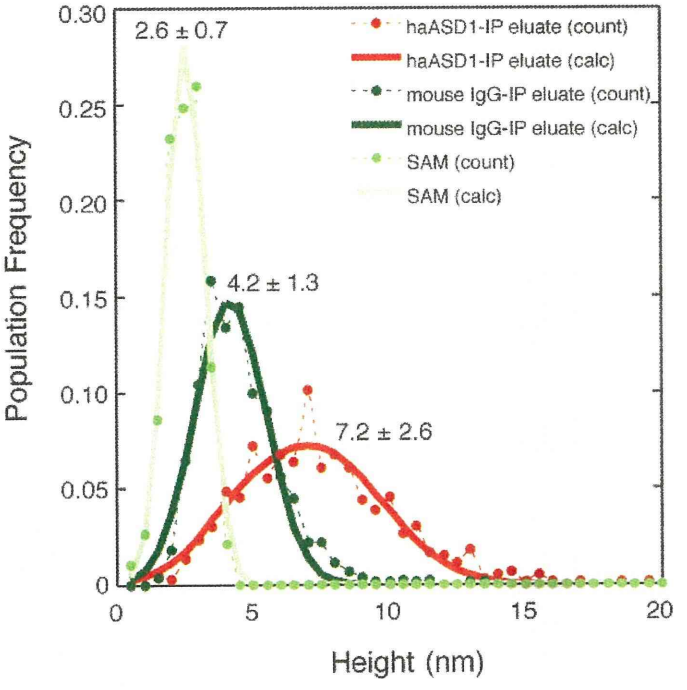

Supplemental Fig. S6. The size of the purified ASPDs. We have previously shown that ASPDs are spheres that have a diameter equal to their height (1) using *in situ* AFM in solution. We therefore determined the size of the purified ASPDs by measuring their height using *in situ* AFM. We examined the height of each structure in anti-ASPD haASD1-immunoprecipitation (IP) eluate (haASD1-IP eluate; n = 591), normal mouse IgG-IP eluate (mouse IgG-IP eluate; n = 759), and self-assembled monolayers (SAMs) on which samples were deposited (SAM; n = 185). Above, the population frequency of the measured height is shown as "count" and that of the fitted data is shown as "calc.". On SAMs, some structures of 2.6 ± 0.7 nm in height were detected. In mouse IgG-IP eluates, ASPD-sized structures were absent, but smaller structures of 4.2 ± 1.3 nm in height were present. These smaller structures were considered to be derived from blocking reagents contained in the elution buffer (Additional Experimental Procedures), since ASPDs and other Aβs were hardly detectable in dot blots using anti-ASPD antibodies (Fig. 2B) or anti-pan Aβ antibodies (2). In contrast, haASD1-IP eluates contained mostly (~94%) spherical structures of 7.2 ± 2.6 nm in height. FCS analysis revealed that the average mass of the unpurified ASPD preparations was 330 ± 58 kDa, while that of the immunoisolated ASPDs was 128 ± 44 kDa. Consistently with this, *in situ* AFM showed that the average height of the unpurified ASPDs was 9.1 ± 2.0 nm (1), while that of the immunoisolated ASPDs was 7.2 ± 2.6 nm.

Downloaded from www.jbc.org at Kyoto University, on March 28, 2011

Fig. S7 Matsumura et al.

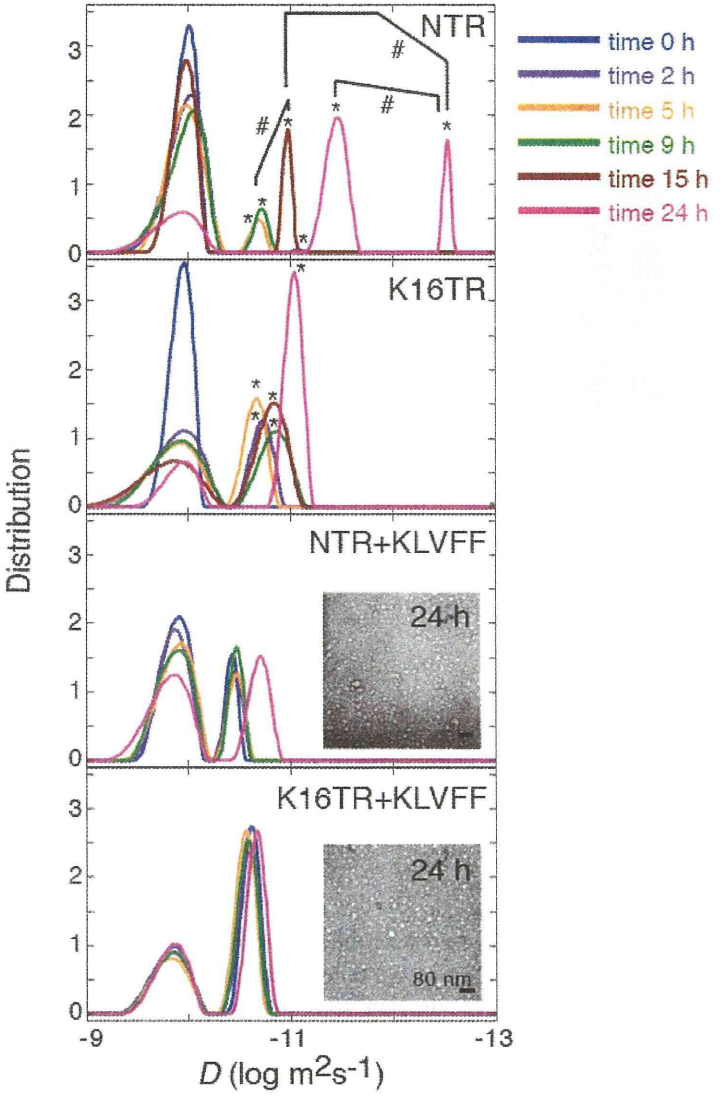

Supplemental Fig. S7. Time course of fibril formation. Fibrils were formed from 100 μM solutions of $A\beta_{1\text{-}40}$ with 0.1 μM NTR or K16TR at pH 3.5. At the onset of fibril formation, a 10-fold molar excess of $A\beta_{16\text{-}20}$ (KLVFF) was added to the $A\beta_{1\text{-}40}$ solutions, and analyses using TEM (*Inset*) and FCS were performed as in Fig. 3 (*, $p < 0.005$ by Scheffé *post-hoc* test compared with the fast-diffusing assembly corresponding to dimers; #, $p < 0.005$ by Scheffé *post-hoc* test). The normalized distribution of assembly diffusion coefficient is shown, as in Fig. 1B.

Downloaded from www.jbc.org at Kyoto University, on March 28, 2011

Fig. S8 Matsumura et al.

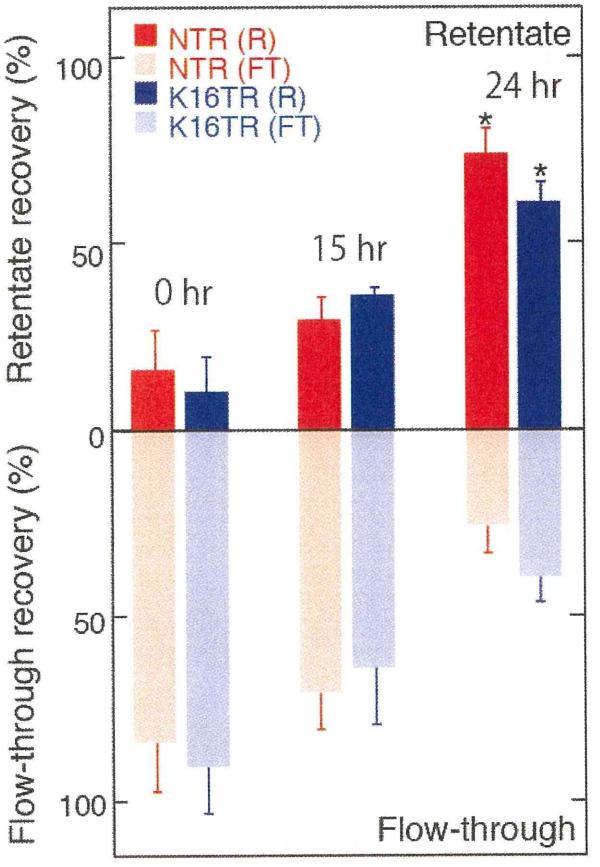

Supplemental Fig. S8. Estimation of fibril amount. We used a probe ratio of 1/1000 for fibrils. To confirm rough estimates calculated from FCS data (see Fig. 3), mature fibrils were separated in the retentate fractions of 0.10-μm filters (confirmed using TEM) and their amount was calculated from the fluorescence count using a fluorometer (Twinkle LB970; Berthold Technologies GmbH; n=5)(mean ± SD; *, $p < 0.005$ by Scheffé *post-hoc* test, n = 6), which was also confirmed by quantitative amino acid analysis (1).

Downloaded from www.jbc.org at Kyoto University, on March 28, 2011

Supplemental References

1. Hoshi, M., Sato, M., Matsumoto, S., Noguchi, A., Yasutake, K., Yoshida, N., and Sato, K. (2003) *Proc. Natl. Acad. Sci. U.S.A.* **100**, 6370-6375
2. Noguchi, A., Matsumura, S., Dezawa, M., Tada, M., Yanazawa, M., Ito, A., Akioka, M., Kikuchi, S., Sato, M., Ideno, S., Noda, M., Fukunari, A., Muramatsu, S., Itokazu, Y., Sato, K., Takahashi, H., Teplow, D. B., Nabeshima, Y., Kakita, A., Imahori, K., and Hoshi, M. (2009) *J. Biol. Chem.* **284**, 32895-32905
3. Wang, H., Chen, S., Li, L., and Jiang, S. (2005) *Langmuir* **21**, 2633-2636
4. Bayburt, T. H., and Sligar, S. G. (2002) *Proc. Natl. Acad. Sci. U.S.A.* **99**, 6725-6730
5. Provencher, S. W. (1982) *Comput. Phys. Commun.* **27**, 213-227
6. Provencher, S. W. (1982) *Comput. Phys. Commun.* **27**, 229-242
7. Widengren, J., Mets, Ü., and Rigler, R. (1995) *J. Phys. Chem.* **99**, 13368-13379
8. Eggeling, C., Widengren, J., Rigler, R., and Seidel, C. A. M. (1998) *Anal. Chem.* **70**, 2651-2659
9. Asimov, M. M., Gavrilenko, V. N., and Rubinov, A. N. (1990) *J. Lumin.* **46**, 243-249
10. Palmer, III, A. G., and Thompson, N. L. (1987) *Biophys. J.* **52**, 257-270
11. Aragón, S. R., and Pecora, R. (1976) *J. Chem. Phys.* **64**, 1791-1803

Downloaded from www.jbc.org at Kyoto University, on March 28, 2011

Supplemental Material can be found at:
http://www.jbc.org/content/suppl/2009/09/15/M109.000208.DC1.html

THE JOURNAL OF BIOLOGICAL CHEMISTRY VOL. 284, NO. 47, pp. 32895–32905, November 20, 2009
© 2009 by The American Society for Biochemistry and Molecular Biology, Inc. Printed in the U.S.A.

Isolation and Characterization of Patient-derived, Toxic, High Mass Amyloid β-Protein (Aβ) Assembly from Alzheimer Disease Brains*[S]

Received for publication, March 2, 2009, and in revised form, September 10, 2009 Published, JBC Papers in Press, September 15, 2009, DOI 10.1074/jbc.M109.000208

Akihiko Noguchi,[a] Satoko Matsumura,[a] Mari Dezawa,[b,c] Mari Tada,[d] Masako Yanazawa,[a] Akane Ito,[a] Manami Akioka,[a] Satoru Kikuchi,[a] Michio Sato,[a] Shouji Ideno,[e] Munehiro Noda,[e] Atsushi Fukunari,[e] Shin-ichi Muramatsu,[f] Yutaka Itokazu,[b] Kazuki Sato,[g] Hitoshi Takahashi,[d] David B. Teplow,[h] Yo-ichi Nabeshima,[b] Akiyoshi Kakita,[d] Kazutomo Imahori,[i] and Minako Hoshi[a,b1]

From the [a]Mitsubishi Kagaku Institute of Life Sciences, Tokyo 194-8511, Japan, [b]Kyoto University, Kyoto 606-8501, Japan, [c]Tohoku University, Sendai 908-8575, Japan, [d]Niigata University, Niigata 951-8585, Japan, [e]Mitsubishi Tanabe Pharma Corporation, Osaka 541-8505, Japan, [f]Jichi Medical University, Tochigi 329-0498, Japan, [g]Fukuoka Women's University, Fukuoka 813-8529, Japan, the [h]David Geffen School of Medicine, UCLA, Los Angeles, California 90095, and [i]University of Tokyo, Tokyo 113-8654, Japan

Amyloid β-protein (Aβ) assemblies are thought to play primary roles in Alzheimer disease (AD). They are considered to acquire surface tertiary structures, not present in physiologic monomers, that are responsible for exerting toxicity, probably through abnormal interactions with their target(s). Therefore, Aβ assemblies having distinct surface tertiary structures should cause neurotoxicity through distinct mechanisms. Aiming to clarify the molecular basis of neuronal loss, which is a central phenotype in neurodegenerative diseases such as AD, we report here the selective immunoisolation of neurotoxic 10–15-nm spherical Aβ assemblies termed native amylospheroids (native ASPDs) from AD and dementia with Lewy bodies brains, using ASPD tertiary structure-dependent antibodies. In AD patients, the amount of native ASPDs was correlated with the pathologic severity of disease. Native ASPDs are anti-pan oligomer A11 antibody-negative, high mass (>100 kDa) assemblies that induce degeneration particularly of mature neurons, including those of human origin, *in vitro*. Importantly, their immunospecificity strongly suggests that native ASPDs have a distinct surface tertiary structure from other reported assemblies such as dimers, Aβ-derived diffusible ligands, and A11-positive assemblies. Only ASPD tertiary structure-dependent antibodies could block ASPD-induced neurodegeneration. ASPDs bind presynaptic target(s) on mature neurons and have a mode of toxicity different from those of other assemblies, which have been reported to exert their toxicity through binding postsynaptic targets and probably perturbing glutamatergic synaptic transmission. Thus, our findings indicate that native ASPDs with a distinct toxic surface induce neuronal loss through a different mechanism from other Aβ assemblies.

Neurodegenerative diseases, such as Alzheimer disease (AD),[2] Parkinson disease, prion diseases, and the polyglutamine diseases, arise from abnormal protein interactions in the central nervous system (1). In these diseases, complex multistep processes of protein conformational change and accretion produce various nonfibrillar assemblies, leading finally to fibrils (1–5). Recent studies have suggested that the early assemblies in this process might be the most toxic, possibly through the exposure of buried moieties and the formation of surface tertiary structures not present in physiologic monomers (6). These surface tertiary structures could mediate abnormal interactions with other cellular components (1).

In AD, extensive studies have suggested that accumulation of amyloid β-protein (Aβ), a physiologic derivative of amyloid precursor protein (APP), plays a primary pathogenic role (7–9). Various forms of assemblies ranging in mass from dimers up to multimers of ~1 MDa have been reported as neurotoxins (10–13) as follows: protofibrils (14); dimers/trimers (natural low-*n* oligomers) (15); 3–24-mer Aβ-(1–42) assemblies termed Aβ-derived diffusible ligands (ADDLs) (16); 12-mers termed globulomers (17) or Aβ*56 (18); 15–20-mer Aβ assemblies termed Aβ oligomers (AβOs) (19); and 150-mer or higher assemblies termed β-sheet intermediates (20). Whether or not they share a common surface, the tertiary structure responsible

* This work was supported in part, by National Institutes of Health Grant NS038328 (to D. B. T.), by Health and Labour Sciences Research Grants "Research on Nanotechnical Medical" (to M. H.) and "Research on Psychiatric and Neurological Diseases and Mental Health" (to M. D.) from the Ministry of Health, Labor, and Welfare, by Special Coordination Funds for Promoting Science and Technology (to M. H.) from the Ministry of Education, Culture, Sports, Science, and Technology, and by the Program for Promotion of Fundamental Studies in Health Sciences (to M. D.) from the National Institute of Biomedical Innovation The authors declare the following conflict of interest: this work was supported in part by a grant (to M. H.) from Mitsubishi Kagaku Institute of Life Sciences, which is a nonprofit organization financially supported by Mitsubishi Chemical Corp.; this grant expires in March 2009.

[S] The on-line version of this article (available at http://www.jbc.org) contains supplemental Experimental Procedures, Tables S1 and S2, Figs. S1–S7, and additional references.

[1] To whom correspondence should be addressed: Sakyo-ku, Kyoto 606-8501, Japan. E-mail: minhoshi@lmls.med.kyoto-u.ac.jp.

[2] The abbreviations used are: AD, Alzheimer disease; Aβ, amyloid β-protein; APP, amyloid precursor protein; sAPPα, human secreted form of APP; ADDL, Aβ-derived diffusible ligand; AβO, Aβ oligomer; ASPD, amylospheroid; DLB, dementia with Lewy bodies; MALDI-TOF/MS, matrix-assisted laser desorption/ionization time-of-flight mass spectrometry; HFIP, 1,1,1,3,3,3-hexafluoro-2-propanol; PBS, Dulbecco's phosphate-buffered saline without Ca^{2+} and Mg^{2+}; TEM, transmission electron microscopy; IP, immunoprecipitation; NCI, noncognitively impaired; MSCs, bone marrow stromal cells; NMDA-R, *N*-methyl-D-aspartate-type glutamate receptor; DIV, days *in vitro*; NCI, noncognitively impaired.

Downloaded from www.jbc.org at Kyoto University, on March 7, 2010

Supplemental Material can be found at:
http://www.jbc.org/content/suppl/2009/09/15/M109.000208.DC1.html

for toxicity remains unsettled; some of these assemblies are detected by specific antibodies (17, 21), whereas others are detected by a polyclonal A11 antibody (18, 19) that is reported to recognize epitopes associated with a certain oligomer state of amyloids regardless of their amino acid sequence (22). However, these assemblies, which differ in origin, mass, and toxic activity, mostly bind to postsynapses, leading to synaptic impairment (17–19, 23, 24). They are also suggested to play a role in synaptic impairment in AD model mice carrying human APP (17, 18, 25), which retain early features of AD such as amyloid plaques, synaptic loss, and mild memory deficits (26, 27). These observations collectively suggest that these assemblies play a role in AD pathogenesis by causing synaptic impairment. On the other hand, it remains largely unknown how, after the synaptic impairment, these assemblies cause subsequent neuronal loss in human AD brains. One reason is that no overt neuronal cell loss has been observed in most APP transgenic mice (except APP23 mice (28, 29)), even in the presence of these assemblies (26, 27). Another reason is that, as for the nonfibrillar Aβ assemblies actually present in human AD brains, Aβ dimers that induce synaptic impairment and not neuronal loss were recently isolated (30), but Aβ assemblies that directly cause neuronal loss have not yet been isolated either from AD patients or from the mice. Because soluble fractions of brains from humans with AD have been reported to contain Aβ assemblies ranging in size from dimers to polymers larger than 100 kDa (31), which appear to correlate with dementia (32, 33), Aβ assemblies responsible for neuronal loss might be present in the soluble fractions of AD brains. As has recently been shown clinically and diagnostically (34–37), neuronal loss plays an important role in cognitive deterioration of AD patients, so we aimed to isolate toxic Aβ assemblies from the soluble fractions of AD brains.

As a first step to isolate such Aβ assemblies *in vivo*, we have previously prepared highly toxic spherical Aβ assemblies termed "amylospheroids" (ASPDs) *in vitro* (38). Notably, ASPDs are considered not to be intermediates in the pathway leading to fibrils, because ASPDs were not incorporated into mature fibrils and continued to exist after fibril formation (13, 38). They also differ from protofibrils and ADDLs in morphology and size (11, 13, 38).

Here, we generated ASPD tertiary structure-dependent antibodies and used them to selectively immunoisolate a human counterpart of ASPDs (native ASPDs) from patients with AD or dementia with Lewy bodies (DLB). To distinguish native ASPDs from *in vitro*-produced ASPDs, the latter is hereafter referred to as synthetic ASPDs. Native ASPDs are A11-negative, high mass Aβ assemblies that induce degeneration of human neuronal cells *in vitro*, particularly those with mature character, and they differ in mass, surface tertiary structure, and neurotoxicity mechanism from other reported nonfibrillar Aβ assemblies (summary in supplemental Table S1).

EXPERIMENTAL PROCEDURES

Aβ Source—Aβ-(1–40) peptides were synthesized using *N*-(9-fluorenyl)methoxycarbonyl (Fmoc) chemistry on an Applied Biosystems model 433A peptide synthesizer and purified (38). Their structure and purity were confirmed using quantitative amino acid analysis, analytic high pressure liquid chromatography, and matrix-assisted laser desorption/ionization-time-of-flight/mass spectrometry (MALDI-TOF/MS; Ultraflex II, Bruker Daltonics). The purified Aβ-(1–40) was lyophilized, dissolved in 35% (v/v) acetonitrile in 0.1% (v/v) trifluoroacetic acid (~50 nmol/tube), and lyophilized. This step was repeated twice. Aβ-(1–42) peptides (25 mg/ampoule; Bachem lots 0552992 and 1000255) were completely dissolved in ~54 ml of 1,1,1,3,3,3-hexafluoro-2-propanol (Aldrich) by incubating the peptide solution overnight at 4 °C and then for 3 h at 37 °C and finally lyophilized (~40 nmol/tube). This step was repeated two or three times. The lyophilized peptides were kept at −20 °C.

Preparation and Purification of Synthetic ASPDs—Synthetic ASPDs were prepared *in vitro* either from 50 μM solution of Aβ-(1–40) (0.5× Dulbecco's phosphate-buffered saline without Ca^{2+} and Mg^{2+} (PBS); Nissui Pharmaceutical Co. Ltd.) or of Aβ-(1–42) (either 0.5× PBS or F12 buffer without L-glutamine and phenol red) by slowly rotating the solution (5–7 days for Aβ-(1–40); 14 h for Aβ-(1–42)), as described previously (38). At concentrations below a critical fibril-forming concentration (~100 μM) (39), spherical Aβ assemblies (5–20 nm in diameter for Aβ-(1–40); 5–25 nm for Aβ-(1–42); >85% 10–15 nm spheres), with rare fibril-like structures, were usually produced. The most toxic ASPDs (prepared either from Aβ-(1–40) or Aβ-(1–42)) were previously identified as 10–15-nm spheres recovered by glycerol gradient centrifugation in the fraction migrating near the thyroglobulin (669 kDa) standard (38). Further analysis of standard proteins using this glycerol gradient sedimentation assay revealed that the mass of the most toxic ASPDs is approximately equal to that of aldolase (158 kDa) but does not exceed that of thyroglobulin (669 kDa).[3] Therefore, the most toxic ASPDs were purified as retentates by using 100-kDa molecular mass cutoff filters (Ultrafree-MC, Millipore) to remove lower mass Aβ assemblies. In some experiments, including mature neuron-binding assays, the most toxic ASPD fraction was also purified by two-step filtrations (see Scheme 1). Studies using transmission electron microscopy (TEM) revealed that 10–15-nm spheres were predominantly recovered in the most toxic ASPD fraction (termed "158–669-kDa ASPDs") that passed through 0.22-μm filters but were retained on 100-kDa molecular mass cutoff filters (data not shown). Although these 10–15-nm spheres were hardly detectable in 100-kDa filtrates, smaller particles with a diameter of 5–6 nm were present in 100-kDa filtrates. A very small amount of 10–15-nm ASPDs was also present in 0.22-μm retentates because they remained bound to the filter (data not shown). These TEM observations were in good agreement with the results of dot blots and toxicity assays shown in Fig. 1*A*. Quantitative amino acid analysis revealed that generally ~25% of total Aβ was recovered as 158–669-kDa ASPDs. Synthetic ASPDs were prepared every week, and their quality was confirmed using dot blotting, TEM, and toxicity assays. Aβ concentration of each preparation was deter-

[3] A. Noguchi and M. Hoshi, unpublished data.

Downloaded from www.jbc.org at Kyoto University, on March 7, 2010

Supplemental Material can be found at:
http://www.jbc.org/content/suppl/2009/09/15/M109.000208.DC1.html

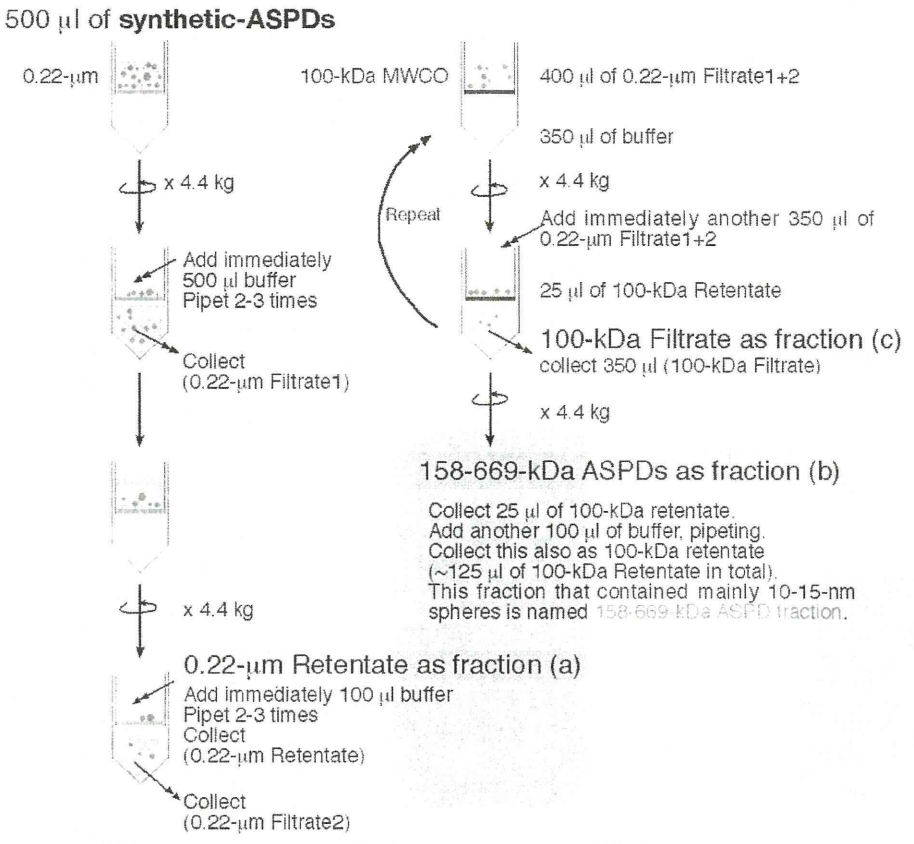

SCHEME 1. **Fractionation of the most toxic 158–669-kDa ASPDs by two-step filtrations.**

mined every week by quantitative amino acid analysis (Waters AccQ-Tag system) (38).

Preparation of Aβ Monomers and Fibrils—To prepare monomers, Aβ-(1–40) or Aβ-(1–42) lyophilizates were solubilized to 50 μM in 1,1,1,3,3,3-hexafluoro-2-propanol. The solution was incubated for 30 min at room temperature and then centrifuged at 20,400 × *g* for 30 min at 4 °C, and the upper 90% of the supernatant volume was collected. The monomer concentration was determined by means of quantitative amino acid analysis (38). To produce fibrils, Aβ-(1–40) was dissolved at a concentration of 100 μM in 0.5× PBS, pH 3.5. This solution was incubated without agitation at 37 °C for 2 days, after which fibrils were separated from the monomer and low mass Aβ assemblies by filtration through 100-kDa molecular mass cutoff filters. Large amounts of fibrils without ASPDs were detected reproducibly by TEM. The fibril concentration was determined by means of quantitative amino acid analysis (38). To obtain different types of fibrils for immuno-TEM analysis, fibrils were also produced by slowly rotating the above Aβ-(1–40) solution or by dissolving Aβ-(1–40) at a concentration of 350 μM in PBS, pH 7.5, followed by incubation for 5–7 days at 37 °C, with or without slow rotation (38).

Preparation of Aβ Oligomers for A11 Antibody—A test membrane, on which soluble Aβ oligomers (termed AβOs) and Aβ fibrils (1–3 μg/dot) were spotted, was produced by Dr. C. Glabe (University of California, Irvine) according to reported methods (22, 40). This test membrane was kindly provided by Invitrogen as a positive control for A11 antibody.

Preparation of ADDLs—ADDLs were produced as described previously (16). Aβ-(1–42) lyophilizates were solubilized to 5 mM in DMSO, diluted to 100 μM with F12, and incubated for 24 h at 4 °C. The solution was centrifuged at 14,000 × *g* for 10 min at 4 °C, and the supernatant was collected. These ADDL preparations were further purified by obtaining the flow-through fraction of 100-kDa molecular mass cutoff filters as described (21).

Human Brain Extracts—The Bioethics Committees and the Biosafety Committees of Mitsubishi Kagaku Institute of Life Sciences, Niigata University, and Kyoto University approved all experiments using human subjects. Freshly frozen brains obtained at autopsy were homogenized to 0.15 g/ml in an ice-cold extraction buffer (either 20 mM Tris-HCl, pH 7.6, 137 mM NaCl, or F12 buffer without L-glutamine and phenol red, containing 1 mM EDTA, 1 mg/ml pepstatin, and complete protease inhibitor mixture (Roche Diagnostics)) using a Potter Teflon/glass homogenizer. Soluble fractions were collected as the supernatant following centrifugation at 104,300 × *g* (TLA100.4) at 4 °C for 1 h. SDS-extractable insoluble fractions were obtained from the pellet by homogenizing in 2% (w/v) SDS and by 1-h gentle shaking at 37 °C, followed by centrifugation for 1 h at 10 °C. Formic acid-extractable fractions were obtained by homogenizing the SDS pellet in 70% formic acid, followed by centrifugation for 1 h. Approximate protein recoveries were 10% for soluble fractions and 90% for insoluble fractions. The possibility of artificial generation of ASPD-like structures from Aβ-(1–42) monomers or of destruction of ASPD-like structures during the extraction procedures was excluded (data not shown). More details are given in the supplemental Experimental Procedures.

Immunoprecipitations (IP)—To remove other assemblies (<100 kDa), soluble extracts from AD or NCI brains were concentrated using 100-kDa molecular mass cutoff filters (Millipore). This process was repeated until we obtained AD-derived 100-kDa retentates that contained native ASPDs at ~10–20 μM; this was verified by dot blotting using rpASD1. IPs were performed using an immunocapturing kit 100 MB-IAC Prot G (Bruker Daltonics), according to the manufacturer's instructions, except that 3% (w/v) bovine serum albumin (Sigma A7030) was used to suppress nonspecific binding. Monoclonal ASD antibodies (haASD1 or mASD3) were used for the immunoisolation because of their high affinity for ASPDs. Captured proteins were eluted using Gentle Elution buffer (Pierce),

Downloaded from www.jbc.org at Kyoto University, on March 7, 2010

Supplemental Material can be found at:
http://www.jbc.org/content/suppl/2009/09/15/M109.000208.DC1.html

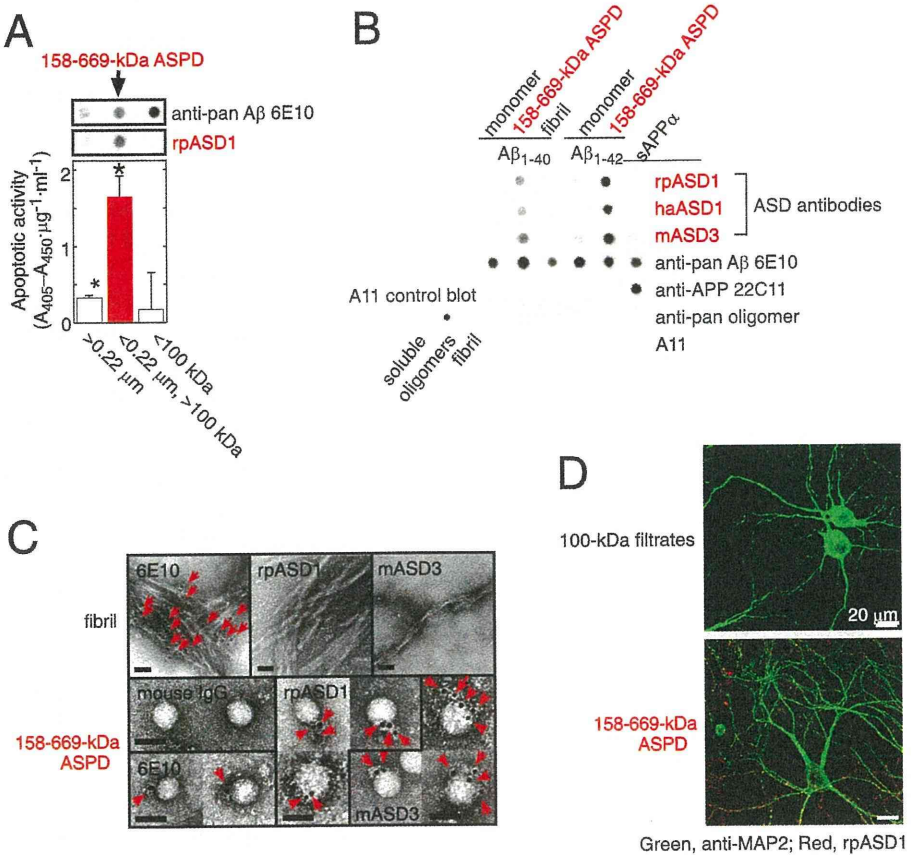

FIGURE 1. **Characterization of ASD antibodies.** *A*, evaluation of two-step filtered fractions (0.22-μm retentates, the 158–669-kDa ASPDs, and 100-kDa filtrates; see Scheme 1 under "Experimental Procedures") by dot blotting using rpASD1 and 6E10 (*upper panel*) and by toxicity assays using rat primary septal cultures (*lower panel*; mean ± S.D.; Games-Howell post hoc test, *, $p < 0.001$, $n = 6$). *B*, dot blotting of Aβ and APP (5 ng/dot). Synthetic ASPDs were prepared *in vitro* either from Aβ-(1–40) or Aβ-(1–42) as described (7). Purified 158–669-kDa ASPD fraction was recovered in 100-kDa retentates as in *A*. Unlike anti-APP-(66–81) (22C11), anti-Aβ-(1–16) (6E10), or A11 antibody, ASD antibodies selectively detected synthetic ASPDs and the 158–669-kDa ASPDs. The control blot membrane for A11 was provided by Invitrogen (supplemental Experimental Procedures). *C*, immuno-TEM analysis. *Arrows* show the secondary antibody-conjugated immunogold. 6E10 detected the 158–669-kDa ASPDs weakly, probably because of its low affinity for synthetic ASPDs. rpASD1 and mASD3 showed little reactivity to fibrils but clearly detected the 158–669-kDa ASPDs. *Bar*, 20 nm. *D*, rpASD1 detected intense signals in 27-DIV mature rat hippocampal neurons treated with the 158–669-kDa ASPDs (in *A*) for 30 min but did not detect signals in those treated with the 100-kDa filtrates containing monomers and Aβ-(1–42) assemblies with mass <100 kDa. Z-stack images are shown (supplemental Experimental Procedures).

because ASPDs retained their structure and toxicity (~100%) after a 60-min exposure to this buffer. The amount of native ASPDs in eluates was immediately examined by dot blotting with polyclonal rpASD1, a suitable antibody for dot blot analysis. Details are given in supplemental Experimental Procedures.

Other Methods—Preparation and screening of ASD antibodies, dot blotting, Western blotting, TEM and immuno-TEM examinations, surface plasmon resonance by Biacore and competitive enzyme-linked immunosorbent assay experiments, pathologic examinations of human brains, *Tg2576* mice experiments, toxicity assays, immunocytochemistry, human neuronal cells, and monkey neural progenitors and neurons, as well as statistics, are described in supplemental Experimental Procedures.

RESULTS

Production and Characterization of ASPD-specific Antibodies—To isolate native ASPDs from AD patients, we raised antibodies against ASPDs in 6 rabbits, 43 mice, and 10 hamsters. As an immunogen, synthetic ASPDs were prepared *in vitro* from 50 μM solutions of Aβ-(1–42) by slowly rotating the solutions for 14 h (38); they included spherical Aβ assemblies of 5–25 nm (>85% of them were 10–15-nm spheres). IgG-class antibodies were purified and named "ASD antibodies," with prefixes indicating the source (rabbit polyclonal as rpASD1; hamster monoclonal as haASD1; mouse monoclonal as mASD3).

We examined the reactivity of ASD antibodies against the most toxic synthetic ASPD fraction separated as follows. Because the mass of the most toxic 10–15-nm ASPDs is almost equal to that of 158-kDa aldolase but does not exceed that of 669-kDa thyroglobulin in sedimentation analysis (38), synthetic ASPDs were further size-separated by means of two-step filtrations (see Scheme 1 under "Experimental Procedures") to concentrate the most toxic 158–669-kDa ASPDs in fraction b, the fraction that passed through 0.22-μm filters but was retained on 100-kDa molecular mass cutoff filters. As expected, 158–669-kDa ASPDs recovered in fraction b included 10–15-nm spheres, as determined by TEM observation (data not shown), and were confirmed to be the most toxic species in toxicity assays (Fig. 1*A*).

Importantly, rpASD1 specifically detected the 158–669-kDa ASPDs in fraction b in dot blotting but had little or no cross-reactivity to fraction a 0.22-μm retentates or fraction c 100-kDa filtrates containing monomers and 5–6-nm particles, which are strongly detected by anti-pan Aβ 6E10 antibody (Fig. 1*A*). We also confirmed that rpASD1 did not cross-react with ADDLs (supplemental Fig. S1*A*). These results indicated that rpASD1 recognizes an epitope that is associated with the most toxic ASPDs but not with ADDLs.

We further characterized rpASD1 and the other ASD antibodies using the most toxic 158–669-kDa ASPDs. As shown in Fig. 1*B*, all ASD antibodies detected primarily the 158–669-kDa ASPDs (prepared from either Aβ-(1–42) or Aβ-(1–40))

Downloaded from www.jbc.org at Kyoto University, on March 7, 2010

Supplemental Material can be found at:
http://www.jbc.org/content/suppl/2009/09/15/M109.000208.DC1.html

TABLE 1

Summary of characters of ASD antibodies and anti-pan Aβ antibodies

The characters of newly established anti-ASPD antibodies (upper three rows) and previously reported anti-pan Aβ antibodies (lower two rows) are summarized. The original epitope mapping data are shown in supplemental Fig. S1*B*; see Fig. 1*A* and supplemental Fig. S3*A* for dot blots and supplemental Table S2 for K_d values determined by Scatchard analysis of enzyme-linked immunosorbent assay data; see Fig. 1*C* (except haASD1) for immuno-TEM and supplemental Fig. S5*A* for toxicity blockade.

Antibody	Preference among Aβ types in dot blotting	K_d for ASPDs	Epitope map	Response to APP in dot blotting	Response to fibrils in immuno-TEM	Blockade of ASPD toxicity
		nM				
rpASD1	ASPD	0.005	Several regions[a]	−	−	+
mASD3	ASPD	0.003	Several regions[a]	±	−	+
haASD1	ASPD	0.0005	Could not be determined[b]	−	−	−
6E10	All types	0.2	Aβ5–9[c]	+	+	−
82E1	All types	ND[d]	Aβ1–5[c]	−	ND	−

[a] The binding of these antibodies to synthetic-ASPDs was most strongly inhibited by N-terminal pentapeptides of Aβ. In addition, the binding was also inhibited by specific sets of non-N-terminal pentapeptides. The data suggest that different Aβ regions exist in close proximity to form the ASPD-specific epitope.

[b] The binding of haASD1 to synthetic-ASPDs was not inhibited by the addition of any pentapeptide, suggesting that haASD1 recognizes a nonlinear epitope formed by noncontiguous Aβ regions.

[c] For 6E10 and 82E1, which did not discriminate ASPDs from other types of Aβ, complete inhibition was attained with a single pentapeptide in each case.

[d] ND means not determined.

but had very low or no cross-reactivity to sAPPα (human secreted form of APP), Aβ monomers, or Aβ fibrils, whereas 6E10 equally detected all these Aβ species and sAPPα (Fig. 1*B*). Consistent with this, ASD antibodies detected 10–15-nm spheres in the 158–669-kDa ASPDs but did not react with fibrils as observed with immuno-TEM under mild fixation conditions (Fig. 1*C*). In accordance with their ASPD preference in dot blots and immuno-TEM, the ASD antibodies showed the highest affinity for the 158–669-kDa ASPDs (K_d 10^{-12}–10^{-13} M; Table 1), rather than for Aβ monomers, fibrils, or sAPPα (supplemental Table S2). These results demonstrated ASPD specificity of all the ASD antibodies. As described above, A11 antibody is a pan-oligomer polyclonal antibody that recognizes epitopes associated with an oligomer state (18, 19, 22). To our surprise, this anti-pan oligomer A11 antibody failed to detect the 158–669-kDa ASPDs (Fig. 1*B*). These results strongly suggested that epitopes recognized by the ASD antibodies are associated with the tertiary structure of ASPDs, which differs from that of A11-positive oligomers, such as Aβ*56 and AβOs, and from that of fibrils. To further elucidate the epitope specificity, we performed epitope mapping by means of competitive enzyme-linked immunosorbent assay using a series of pentapeptides covering the entire Aβ-(1–42) sequence. As summarized in Table 1, no single pentapeptide could compete out binding of the ASD antibodies to the 158–669-kDa ASPDs, suggesting that different Aβ regions exist in close proximity within ASPDs to form ASPD tertiary structure-dependent epitopes that are not present in a single Aβ monomer (supplemental Fig. S1*B*). The ASD antibodies produced only weak or no bands in Western blots under denaturing conditions (data not shown), as would be expected from the fact that they recognize ASPD tertiary structure. We finally examined whether the ASD antibodies are available for detecting ASPDs bound to mature neurons, because we have previously shown that synthetic ASPDs directly induce neuronal cell death, possibly by binding to neuronal cell surfaces (38). As shown in Fig. 1*D*, the ASD antibodies clearly detected synthetic ASPDs bound on mature rat hippocampal neurons (see "Experimental Procedures") when the neurons were briefly treated with the 158–669-kDa ASPDs and fixed under mild conditions, but they did not label neurons treated with the 100-kDa filtrates, which contained monomers and 5–6-nm particles of less than 100 kDa. The characteristics of the antibodies are summarized in Table 1. All of these results demonstrate that the ASD antibodies recognize epitopes that are specific to the surface tertiary structure of ASPDs, which differ from that of ADDLs, A11-positive prefibrillar oligomers, and fibrils.

ASPD-specific Antibody-stained AD Brain—To elucidate whether synthetic ASPD-like assemblies are present *in vivo*, brain sections of patients with clinico-pathologically confirmed AD (41) (n = 10; age 80.4 ± 9.2 years, brain weight 964 ± 82 g, disease duration 10.1 ± 5.5 years) and those of NCI people (n = 7; age 71.3 ± 15.2 years, brain weight 1226 ± 96 g) were immunostained with ASD antibodies. The reactivity of the ASD antibodies in AD patients was strongly associated with brain regions where prominent neurodegeneration had occurred (*e.g.* temporal cortex, frontal cortex, and hippocampus) (Fig. 2*A* and supplemental Fig. S2) but was rarely observed in NCI brains (data not shown). This immunoreactivity in AD brains was associated mainly with plaques and occasionally with neurites and some microvessels and was eliminated by prior treatment of the ASD antibodies with the 158–669-kDa ASPDs (data not shown).

We next compared the reactivity to plaques under various conditions between the ASD antibodies and anti-pan Aβ antibodies, the most widely used antibodies for detecting fibrils in plaques. Although anti-pan Aβ antibodies labeled plaques only in formalin-fixed paraffin sections after pretreatments such as microwaving or formic acid, ASD antibody-specific reactivity was observed most strongly in cryosections and more weakly in formalin-fixed paraffin sections with or without pretreatments (except that haASD1 is available only for cryosections) (Fig. 2*A*). This difference in immunoreactivity to plaques suggested that anti-pan Aβ antibodies and ASD antibodies detect different structures in plaques; anti-pan Aβ antibodies detect fibrils when buried epitopes are exposed by protein-denaturing treatments, whereas ASD antibodies are considered to detect tertiary structure-dependent epitopes on putative human ASPD counterparts under conditions where the native structure of proteins is preserved. To confirm this, we performed biochemical fractionation of AD brains and examined whether these antibodies reacted with insoluble or soluble fractions. Consistent with previous data that fibrils include an insoluble core of plaques (42), anti-pan Aβ antibodies reacted mainly (>85%)

Downloaded from www.jbc.org at Kyoto University, on March 7, 2010

Supplemental Material can be found at:
http://www.jbc.org/content/suppl/2009/09/15/M109.000208.DC1.html

Isolation of Toxic High Mass Aβ Assembly from AD Patients

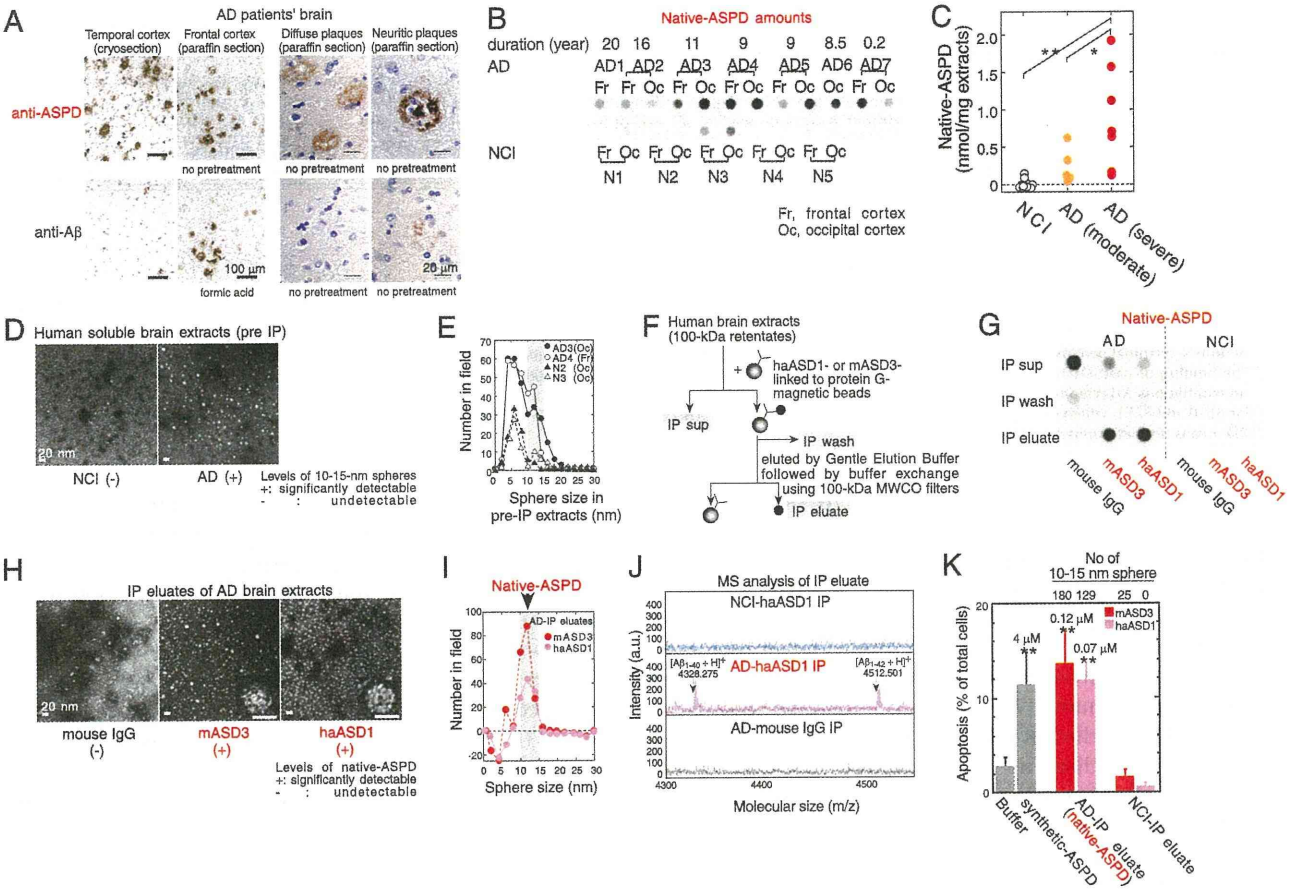

FIGURE 2. **Isolation of native ASPDs.** *A*, AD brains were stained with rpASD1 (5 μg/ml) or anti-Aβ1–42 C-terminal antibody (0.5 μg/ml; 2 μg/ml for cryosections). *B* and *C*, dot blotting of 100-kDa retentates (>100 kDa) of AD or NCI brain extracts (1 μg of soluble extracts/dot) using rpASD1 (Scheffé post hoc test; **, $p = 0.0011$; *, $p = 0.0388$). *Fr*, frontal cortex; *Oc*, occipital cortex. *D* and *E*, TEM images (*D*) and particle analysis of 100-kDa retentates ($n = 3$; 10 randomly selected fields) (*E*). *F* and *G*, method for immunoprecipitation (*IP*) (*F*) and dot blotting (using rpASD1) of IP supernatants (*sup*), wash, and eluate fractions. IPs were performed using haASD1, mASD3, or mouse IgG (*G*). *H* and *I*, TEM images (*inset, bar*, 10 nm) (*H*) and particle analysis of IP eluates ($n = 3$; 15 randomly selected fields, background (a small amount of spheres <10 nm contained in eluate with buffers)-subtracted data are shown) (*I*). *J*, representative MALDI-TOF/MS data. Aβ-(1–40) and Aβ-(1–42) were detected only in native ASPDs at theoretical monoisotopic mass values ($([A\beta\text{-}(1\text{–}40) + H]^+$, 4328 Da; $[A\beta\text{-}(1\text{–}42) + H]^+$, 4512 Da) as observed in synthetic Aβ peptides. *K*, toxicity of isolated native ASPDs toward primary rat septal neurons (mean ± S.D.; Scheffé post hoc test, **, $p < 0.0001$, compared with buffer, $n > 8$) correlated with the 10–15-nm sphere number determined as in *I*. Neurons treated with NCI-IP eluates showed only background levels of apoptosis similar to those of neurons treated with buffers. *Inset*, synthetic or native ASPD amounts in Aβ monomer concentrations.

with insoluble fractions of AD brains extracted with SDS or formic acid (supplemental Fig. S3*A*). Furthermore, this insoluble fraction produced broad smears in Western blots of Aβ, as is usually observed with fibrils (42) (supplemental Fig. S3*B*). In contrast, the ASD antibodies reacted only with soluble fractions of AD brains (supplemental Fig. S3*A*) in which the human ASPD counterpart was actually present, as described below (see under "Isolation of Native ASPD from Brains of AD Patients"). These results collectively indicate that the ASD antibodies detect a human ASPD counterpart, namely native ASPD, associated with plaques and neurites in AD brains. In subsequent work, we used monoclonal mASD3 and haASD1 for isolating ASPDs, because of their high affinity, and polyclonal rpASD1 for detecting ASPDs (except Fig. 3*A*; see also "Immunoprecipitations" under "Experimental Procedures").

Isolation of Native ASPD from Brains of AD Patients—The tissue fractionation study revealed that native ASPDs are recovered in soluble fractions of AD brains. To investigate the amount of native ASPD, we prepared soluble fractions of AD brains ($n = 7$; age 85.6 ± 3.1 years, brain weight 1025 ± 104 g) and NCI ($n = 5$; age 72.6 ± 9.5 years, brain weight 1236 ± 64 g) by means of a nondenaturing procedure using solutions of physiologic ionic strength and pH without detergents. We then obtained 100-kDa retentates of the soluble fractions to concentrate native ASPDs (larger than 100 kDa) and to eliminate other Aβ assemblies smaller than 100 kDa (as performed in Fig. 1*A*). The 100-kDa retentates of AD brains thus obtained had high levels of rpASD1-reactive substances, but those of NCI brains had very low or negligible reactivity (Fig. 2*B*). Consistent with the above data, much higher numbers of spheres sized 10–15 nm were present in 100-kDa retentates of AD patients than in those of NCI (Fig. 2, *D* and *E*). These results suggest that rpASD1-reactive 10–15-nm spheres in 100-kDa retentates of AD are native ASPD candidates. We then immunoisolated native ASPDs (Fig. 2*F*) from large amounts of AD-derived 100-kDa retentates using two monoclonal antibodies, haASD1 and mASD3 (Fig. 2, *G–J*). These antibodies were chosen for their extremely high affinity for ASPD ($K_d < 10^{-12}$ M) and for their

Downloaded from www.jbc.org at Kyoto University, on March 7, 2010